Generating Ultrastable Glasses by Homogenizing the Local Virial Stress

Fabio Leoni,[1,*] John Russo,[1] Francesco Sciortino,[1] and Taiki Yanagishima[2,†]
[1]*Department of Physics, Sapienza University of Rome, Piazzale Aldo Moro 5, 00185 Rome, Italy*
[2]*Department of Physics, Graduate School of Science, Kyoto University, Kyoto 606-8502, Japan*

(Received 18 July 2024; accepted 19 February 2025; published 25 March 2025)

The algorithmic preparation of ultrastable glasses (UG) has considerably expanded our understanding of the glassy state. In this work, we report on a new protocol for UG preparation in a model colloidal glass that iteratively modifies particle diameters to reduce local virial stress fluctuations, effectively homogenizing the local mechanical environment of individual particles. We apply the algorithm to an additive Lennard-Jones mixture and show that, compared to the states obtained via thermal annealing, virial homogenized glasses are characterized by a considerable increase in both kinetic stability and the number of locally favored structures, and melt during heating ramps via an accumulation of localized events. Our results show that microscopic mechanical homogeneity, a widely applicable concept, can give rise to ultrastability.

DOI: 10.1103/PhysRevLett.134.128201

Since pioneering work by Ediger and collaborators [1], the advent of ultrastable glasses has opened new frontiers in the application and the understanding of glassy materials [2,3]. They are defined by an enhanced kinetic and thermodynamic stability with respect to glasses annealed on experimental timescales; in experiment, they are commonly obtained from vapor deposition on a substrate at a certain temperature and deposition rate [3]. The same stability would require thousands of years of aging when starting with annealed glasses [4]. Recent investigations have shown that the use of sample size effects [5,6] or "hyperaging" of systems with a glass transition just above room temperature [7] may also be feasible strategies. The enhanced stability of ultrastable glasses is reflected in many properties [3,8–12]: these include resistance to permeation by inert gas [2], resistance to crystallization [3,13], the ability to modulate chemical reactivity [14], and resistance to devitrification [2]. Promising applications of this technology include the realization of organic light emitting diode displays [2], the stabilization of amorphous pharmaceuticals [2], the miniaturization of computing components [15–19], and improved mechanical properties in metallic glasses [20–22].

At the same time, numerical simulations which reproduce these experiments, especially vapor deposition [2,3,23–25], have yielded important insights into the mechanism underlying ultrastable glass formation. The timescales accessible, however, prevent reproduction of the same degree of stability [4,24,26]. In order to reach the same levels of ultrastability as those displayed in experiments, simulations have exploited preparation routes based on unphysical moves. The most successful so far are swap moves [27–29], where particles are free to swap positions. Swap has proven to be effective in equilibrating size polydisperse mixtures well below the conventional (without swap) glass transition temperature [27,30,31]. Swap simulations close to the glass transition temperature have shown that relaxation is initially localized, and that successive events take place close to the original ones, which point toward a dynamic facilitation as the main ingredient for the dynamics at deeply supercooled conditions [32] and are responsible for the asymmetric wings observed in experimental relaxation spectra [33]. The greatest strength of the swap algorithm can also, in some applications, be its biggest weakness as its remarkable equilibration ability often leads to the crystallization of the system unless tailored size distributions are used [27]. Other unphysical moves that promote the formation of ultrastable glasses have been introduced, such as the random bonding of monomers [34,35], random pinning of particles [36,37], or changing particle diameters [30,38–42] to minimize the potential energy with some population constraint.

Recently, a new move which changes the particle sizes in a monodisperse repulsive system to even out local densities was shown to produce weakly polydisperse glasses resistant to devitrification [43]. These microscopically density "uniform" glass states did not show any aging within the timescales simulated, in contrast to the intermittent dynamics seen in quenched glasses prepared with the same particle size distribution [44,45] and enhanced resistance to crystallization when placed adjacent to a crystal [46]. Analysis of uniform glasses revealed a homogenization in the number of load-bearing nearest neighbors for each particle, suggesting that homogenization of local mechanical environments might be used to produce more stable glasses.

In this work, we aim to show that mechanical homogenization is not simply an emergent feature of stable states

---

[*] Contact author: fabio.leoni@uniroma1.it

[†] Contact author: yanagishima.taiki.8y@kyoto-u.ac.jp

but may be applied as a direct means to achieve glass stabilization. While homogenizing local densities applies to monodisperse or weakly polydisperse systems [43], it could not be applied to multicomponent systems: this is a prohibitive roadblock to stabilizing widely studied model glasses. Specifically, we propose an algorithm that homogenizes local virial stress of the inherent structure of a glass by incremental changes to individual particle sizes. The algorithm acts on the configurational part of the pressure tensor: as the distribution of virial stresses sharpens, this progressively reduces both the bulk pressure and the energy of the system without necessarily reaching an equilibrium state.

We will show that, for an additive Lennard-Jones mixture, our algorithm produces ultrastable glasses with a considerable increase in the thermodynamic and kinetic stability of the system with respect to conventional glasses quantified by the potential energy and onset temperature. Moreover, we will show that the increased stability is associated with a drastic increase in the number of locally favored structures, confirming the link between ultrastability and structural properties that was recently introduced in Ref. [25]. Finally, we will show that melting dynamics emerge through a cascade of localized events, similar to what was recently discovered in deeply supercooled states [32,36,47–49]. Note that our method is not an equilibration procedure and does not maintain detailed balance. We focus on nonequilibrium melting dynamics; and yet, as will be shown, we have achieved stabilization similar to those reached by the above equilibration techniques.

Methods—Virial homogenized glasses (VHGs) are produced using an iterative scheme as illustrated in Fig. 1(a). Briefly, we start from a supercooled configuration cooled to some temperature significantly below the glass transition temperature, where the inherent structure is no longer strongly temperature dependent. For the Wahnström system, we choose $T = 0.1$. Here, first, we find the inherent structure; this is our starting point. Then, we compute local excess pressure contributions $P_{2,i}$, apply modifications to particle sizes to bring the local $P_{2,i}$ closer to the mean, and find the inherent structure. The new structure is accepted if the standard deviation $\Delta P_{2,i}$ in the distribution of excess pressures is reduced, and rejected if not. If rejected, modifications are made smaller, and the process is repeated. Details are provided in the End Matter. The action of the algorithm can be traced by following distributions over iterations. For example, the distribution of $P_{2,i}$ is seen to sharpen significantly, as shown in Fig. 1(b); the standard deviation in $P_{2,i}$ is reduced by an order of magnitude by the end. The final size distribution is significantly wider than the original binary configuration, as shown in Fig. 1(c), but it is still possible to tell the two species apart. We also confirm that despite some modification, the local Voronoi volume fraction ϕ_i still has two peaks, as shown in Supplemental Material [50].

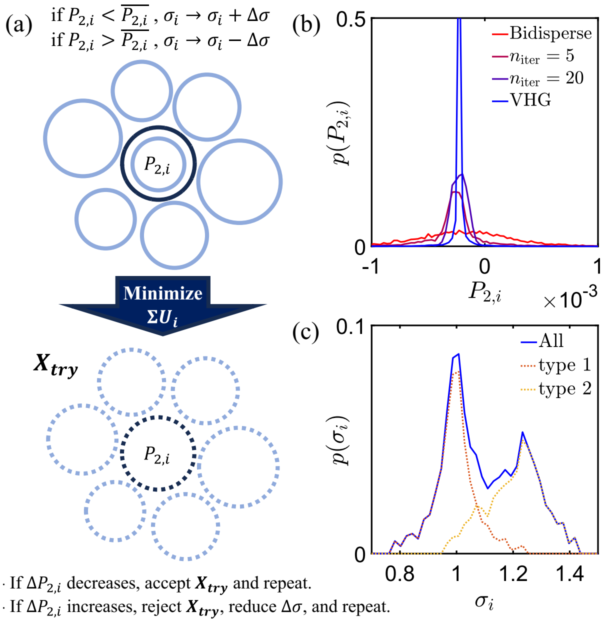

FIG. 1. Creation of "virial homogenized" glasses (VHGs). (a) Illustration of the iterative scheme used to make VHGs for a move where $dP_{2,i}/d\sigma_i > 0$. (b) The distribution of local virial pressures $P_{2,i}$ with iteration. (c) The size distribution σ_i obtained after producing a VHG from the Wahnström (binary Lennard-Jones) glass.

The system we consider is a smoothed version (WAHNs) of the equimolar additive Lennard-Jones binary mixture introduced by Wahnström (WAHN) [52] (see Supplemental Material [50]). This potential has been used to model metallic glasses and represents a good model system to monitor and correlate microscopic structural properties with the thermodynamics of the material [52–57]. All simulations are run with the LAMMPS molecular dynamics package [58] at constant volume. In the following, we report results in reduced units (energy in unit of ϵ, distances in unit of σ, temperature in units of ϵ/k_B).

Results and discussion—Stability: We start by cooling a bidisperse smoothed Wahnström mixture from $T = 1.0$ to $T = 0.1$ with a cooling rate of $\gamma = \Delta T/\Delta t = 1.8 \times 10^{-7}$ corresponding to a change of $\Delta T = 0.9$ in 10^9 integration steps ($dt = 0.005$ in reduced units). The potential energy during the cooling is plotted as an orange curve (overlapped by the black curve) in Fig. 2(a), where a supercooled liquid state is observed for $T \gtrsim 0.55$ followed by an out-of-equilibrium glassy state at $T \lesssim 0.55$. At low T, there is a linear dependence on temperature with a slope approaching the value $3k_BT/2$, showing that the state is trapped in an essentially harmonic well.

At the end of the cooling ramp we take the last configuration and produce a VHG state. Then, we test the kinetic stability of both these configurations (before and after the homogenization algorithm) by heating them at a

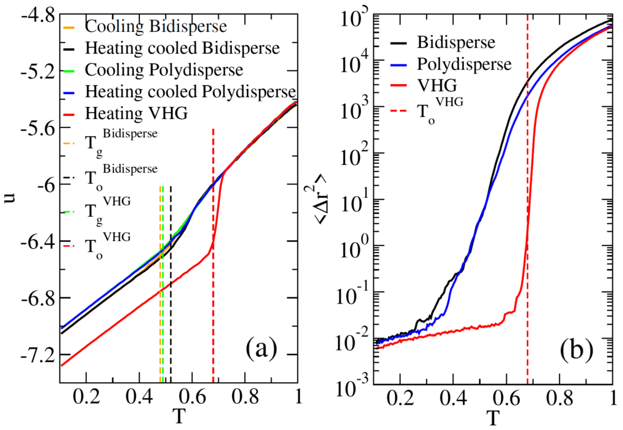

FIG. 2. Enhanced thermodynamic and kinetic stability of VHG states. (a) Potential energy per particle vs T for bidisperse, polydisperse (obtained by melting and cooling VHG), and VHG systems. Vertical dashed lines indicate estimations of T_g and T_o (see text). Note that the orange line almost coincides with the black line. (b) Squared displacement of particles, comparing heating ramps of bidisperse, polydisperse, and virial homogenized glasses. $\langle \Delta r^2 \rangle$ is the squared displacement of particles from their positions at $T = 0.1$ during each ramp.

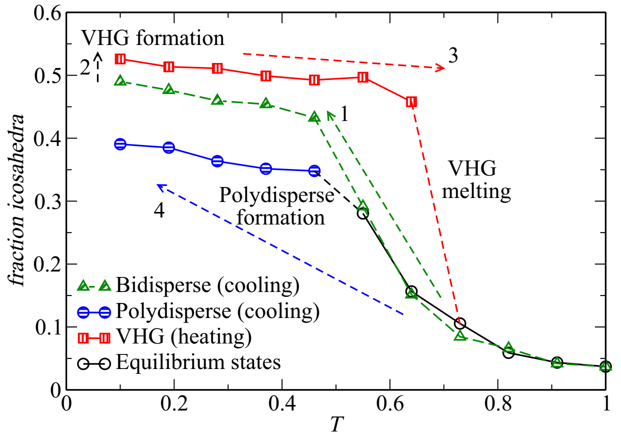

FIG. 3. Fraction of icosahedra vs T for the following systems: cooling of the bidisperse system (green) and the polydisperse melt (blue), heating of VHG (red), and the liquid at equilibrium (black).

heating rate γ. The heating curves are reported in Fig. 2(a) with a black and red line for the configuration before (bidisperse) and after (VHG) the homogenization algorithm. For the original bidisperse mixture, there is very little difference in energy between cooling and heating (orange and black curves, respectively). In contrast, not only is the VHG state (red curve) lower in energy, it shows significantly enhanced kinetic stability, staying glassy up to higher temperatures (more details to follow).

To exclude the possibility that the exceptional stability of the VHG glass is trivially due to its polydispersity, we melt the VHG glass to $T = 1$ and produce an annealed glass at the same cooling rate γ as for the bidisperse system. This cooling curve is shown in green in Fig. 2(a), labeled "polydisperse": the curve almost exactly mirrors the behavior of the original bidisperse glass. This confirms that the stability of the VHG state is not associated with its size distribution, but from its position in a deep minima of the potential energy landscape which is not accessible via standard annealing.

In Fig. 2(b), we consider the dynamics of the three different systems (bidisperse, polydisperse, and VHG) during the heating ramps by plotting the mean square displacement $\langle \Delta r^2 \rangle = 1/N \sum_{i=1}^{N} [r_i(T) - r_i(T = 0.1)]^2$ of all N particles compared to their starting state at $T = 0.1$. In agreement with the results obtained in Fig. 2(a), we observe that the glass melting of the VHG system is more sharp and occurs at considerably higher temperatures.

From the intersection between the glass line and the supercooled line in Fig. 2(a), we may estimate the glass transition temperature T_g for each model. We find $T_g^{\mathrm{bidisperse}} = 0.48$ and $T_g^{\mathrm{VHG}} = 0.49$. The onset of melting is found in Fig. 2(b), where the mean squared displacement $\langle \Delta r^2 \rangle$ versus T undergoes a sudden increase $[T(\langle \Delta r^2 \rangle \simeq 1)]$. We find $T_o^{\mathrm{bidisperse}} = 0.52$ and $T_o^{\mathrm{VHG}} = 0.68$. Note that the displacement of T_o from T_g is a common metric for characterizing ultrastable states [2,3]. Here, we find $T_o^{\mathrm{VHG}} / T_g^{\mathrm{VHG}} = 0.68/0.49 = 1.39$. This is significantly larger than what is usually obtained with vapor deposition, even though we expect this ratio to decrease for a lower γ, approaching typical experimental values. For reference, the typical value obtained for vapor deposited organic molecules is $T_o/T_g \sim 1.05$ [2].

Locally favored structures: Both the fragility and the dynamic heterogeneities of the Wahnström system have been linked with an increase in the number of icosahedral environments that form around the small particles [52–57]. In the glass phase, both the composition and relative orientation of the icosahedra are disordered and distinct from those found in the crystalline structure (the Laves phase A_2B [56]). A similar correlation has recently been found in a vapor deposited ultrastable glass of Wahnström particles [25], where the fraction of icosahedral environments was linked with its stability. Thus, we study the population of icosahedral environments in VHG glasses, identifying icosahedra with the Voronoi topology based tool VoroTop [59]. Figure 3 shows the fraction of icosahedra with respect to the small particles (which in the original Wahnström model have a diameter of σ_{11} and make up half of the total) versus temperature. We consider the cooling of the original bidisperse system, the VHG state during melting, and cooling of the same polydisperse particle population all performed at the same rate γ. Characterization of equilibrium liquid configurations are also presented for comparison. While increasing polydispersity usually disrupts icosahedral environments, the first surprising result is that the homogenization procedure produces a higher fraction of icosahedral environments, despite the increased polydispersity. If we compare the polydisperse system and the VHG state, which have the same size distribution, the contrast is even stronger. We stress that this does not correspond to crystallization; no spatial correlations are seen in the positions of icosahedra (see Supplemental Material [50]). These results confirm that there is a strong link between glass stability and the fraction of icosahedral environments, and that VHG states are thermodynamically, kinetically, and structurally more stable.

Relaxation dynamics: From the curve of the mean squared displacement of the VHG glass in Fig. 2(b), we notice that during heating, the system moves from a frozen to a diffusive regime through a steplike dynamics around temperatures in the range $0.6 \leq T \leq 0.65$. This suggests the presence of avalanchelike behavior during glass melting [44,45]. In the inset of Fig. 4(a), we plot the logarithm of the displacement of all particles in the VHG state during the heating ramp, where we observe the presence of a population of particles which exhibit occasional jumps before the melting temperature, on the order of a particle diameter. In Fig. 4(a), we plot the histogram of the logarithm of displacements measured at three different temperatures. At $T = 0.65$ (in black), two populations of particles can be distinguished based on their displacement Δr from the initial configuration: a large population with small Δr forming the left peak corresponding to the particles that are trapped in their cages and exhibit only vibrational motion and a (very) small population of particles that undergo displacement comparable to the particle size ($\Delta r \approx 1$). At $T = 0.7 > T_g^{\mathrm{VHG}}$ (in red) the fast peak already comprises the majority of particles, while at $T = 0.75$ (in blue) all particles have diffused several particle diameters.

Thus, melting of the bulk ultrastable glass occurs via a well-defined population of particles with intermittent (avalanchelike) dynamics. In Fig. 4(b), we plot the trajectories of all particles during the heat ramp for the temperature range going from $T = 0.6$ to $T = 0.675$: trajectories where the particle has moved less than two particle diameters are given in gray, while more mobile particle trajectories are shown in color. It is clear that the fast particles are spatially correlated and appear in compact regions. These results confirm the presence of localized fast regions [47] and that glass melting is akin to a nucleation-and-growth process [48].

By computing the change in the displacement δ^* undergone by each particle over the temperature range $T =$ 0.6–0.65 where the system changes dynamical regime [$\delta^* = \Delta r(T = 0.65) - \Delta r(T = 0.60)$, $\Delta r(T) = |\mathbf{x}(T) - \mathbf{x}(T = 0.1)|$], we can distinguish a subset of particles displacing at larger distances with respect to the rest of the system. The value of δ^* separating these two subsets of particles is conveniently fixed to 0.3 (see Supplemental Material [50]). On considering the mobile fraction, there is a clear correlation between larger displacement and small particle size (see Fig. S2 in Supplemental Material [50]). Furthermore, from Fig. 4(c), we can see a slice of the box including particles with $\delta^* > 0.3$ which are found in regions of the system free of icosahedra (indicated in gray). This shows that glass melting starts in regions devoid of locally favored structures.

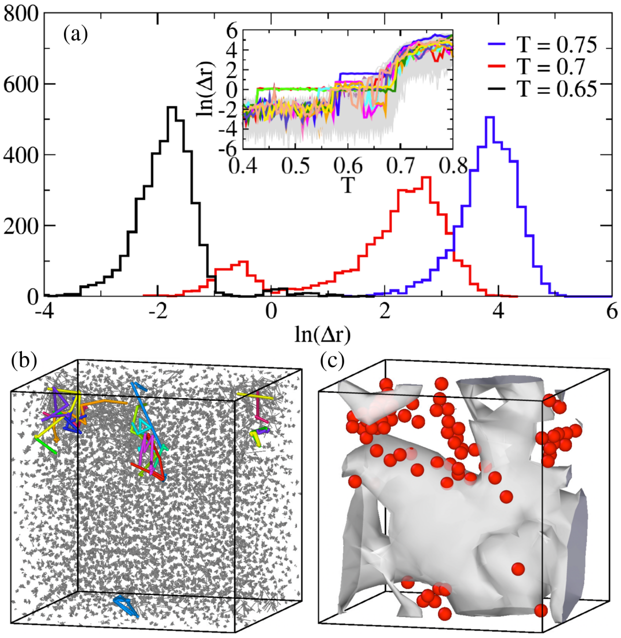

FIG. 4. (a) Histogram of the logarithm of displacements during the heating ramp of the VHG system at three specific temperatures, $T = 0.65$, 0.70, 0.75. There are two populations, corresponding to caged (left peak) and diffusing (right peak) particles. At $T = 0.75$ no more particles are caged. Inset: Logarithm of the displacement vs T for all particles during the heating ramp (full T range is given in Supplemental Material [50]) applied to the VHG system. Around $T = 0.6$ diffusing particles (with $\Delta r > 1$) start to appear. (b) Trajectories of all particles of the VHG system during the heating ramp taken from $T = 0.6$ to $T = 0.675$. Gray trajectories show particles whose displacement at $T = 0.65$ is less than two starting from the $T = 0.6$ state. Particles where $\Delta r > 2$ are plotted in color. (c) Slice through VHG at $T = 0.65$ during heating ramp showing particles with variation of the displacement $\delta^* > 0.3$ (red) and regions where there are icosahedra.

Discussions and conclusions—While there are no direct analogs to VHG glasses, we note that their stability is consistent with previous work considering heterogeneity in local mechanical environments in glasses. For example, it has been shown that a heterogeneous local elasticity can give rise to a Boson peak in the vibrational density of states in molecular glasses [60,61] as well as in jammed packings [62,63]. The presence of excess modes may be interpreted as a "softening" of the material, though evidence to link this to nonequilibrium melting remains a topic of active debate (see, e.g., [64,65]).

We note that it may be possible to encapsulate the VHG approach by direct adjustment of a Hamiltonian. Previous work [30] studying swap dynamics has defined a thermodynamic approach with a conventional interparticle Hamiltonian but with particle size as an evolving variable. In principle, it would be possible to use this as a starting point and add a Hamiltonian term that penalizes variance in nearest-neighbor virial stress. We note that the coupling between the elimination of virial stress fluctuations and energy in our system may be a product of the strong coupling between virial stress and local energy for Lennard-Jones states [66]. Indeed, if this is the case, then the ultrastability from VHG may be a common character shared between a whole family of "isomorphic" systems.

We also briefly consider how numerical studies like this might inform the experimental realization of ultrastable colloidal packings. Though evidence of suppressed particle dynamics has been reported for two-dimensional systems [67], the experimental realization of bulk ultrastable colloidal glasses remains difficult. The single particle editing required for swap or the VHG protocol would be impractical. The random bonding suggested by Ozawa *et al.* [34] could be realized using particles with directional interactions, but it is unclear whether this would be a route of choice for arbitrary particle populations However, our work suggests that the homogenization of mechanical environments itself might be an effective route to improving the stability of glasses, given an appropriate annealing procedure. Despite there being no reports of ultrastability through annealing alone as of yet, mechanically or thermally annealed states do show some of the hallmarks of a more equilibrated glass, such as brittle fracture [68,69], and reduced energy or enhanced modulus [70]. Heterogeneity in local elasticity in metallic glasses as expressed by a heterogeneous local yield stress, has been shown to lead to material softening (as reviewed in [71]): this suggests that their removal would yield the hardest, most equilibrated glass. The feasibility of annealing to produce mechanical homogeneity and ultrastability remains a topic for future work.

To summarize, we explored a new protocol for the preparation of ultrastable glasses, an algorithm that homogenizes local virial stress fluctuations. Applying this algorithm to an additive Lennard-Jones mixture, we observed significant improvements in the thermodynamic, kinetic, and structural stability of the glass. Thermodynamic stability is seen in a sharp decrease in the potential energy of the system. Kinetic stability was observed in a considerable increase in the onset or melting temperature of the glass and in the transition becoming more sharp. Structural stability was inferred by a strong increase in locally favored structures, which, for this system, are the icosahedral environments. Then, we considered the melting behavior of the ultrastable glass, finding that bulk melting starts from localized regions devoid of icosahedral ordering. The motion in these regions is characterized by avalanche-like intermittent motion of a small number of particles with a lower than average radius, which then trigger the melting of the rest of the glass. There is also an interesting converse question regarding whether existing ultrastable glass states (e.g., generated using the swap algorithm) bear any of the hallmarks of VHG states, particularly given that most existing ultrastable states are equilibrium states while VHG states are not. We present a preliminary analysis as End Matter, and leave a more detailed discussion for future work.

Our results provide strong evidence for a deep link between thermodynamic and mechanical stability of ultrastable glasses. The observed virial stress homogenization, in addition to the well-established link between stability and the fraction of icosahedral structures, provides valuable insights into the mechanisms governing glass stabilization. In this respect, the regions with virial stress heterogeneity can be seen as mechanical defects whose suppression considerably increases the thermodynamic stability of the ultrastable state, i.e., the height of the energy barriers that separate it from nearby minima.

Acknowledgments—F. L. and J. R. acknowledge support from the European Research Council Grant No. DLV-759187. F. L., J. R., and F. S. acknowledge support by ICSC–Centro Nazionale di Ricerca in High Performance Computing, Big Data and Quantum Computing, funded by European Union–NextGenerationEU, and CINECA-ISCRA for HPC resources. T. Y. acknowledges the Kyoto University Foundation, support through JST CREST Grant No. JPMJCR2095 and JSPS KAKENHI Grant No. 24K00597.

[1] S. F. Swallen, K. L. Kearns, M. K. Mapes, Y. S. Kim, R. J. McMahon, M. D. Ediger, T. Wu, L. Yu, and S. Satija, Science **315**, 353 (2007).
[2] M. D. Ediger, J. Chem. Phys. **147**, 210901 (2017).
[3] C. Rodriguez-Tinoco, M. Gonzalez-Silveira, M. A. Ramos, and J. Rodriguez-Viejo, Riv. Nuovo Cimento **45**, 325 (2022).
[4] I. Lyubimov, M. D. Ediger, and J. J. de Pablo, J. Chem. Phys. **139**, 144505 (2013).
[5] X. Monnier, J. Colmenero, M. Wolf, and D. Cangialosi, Phys. Rev. Lett. **126**, 118004 (2021).
[6] V. Di Lisio, I. Gallino, S. S. Riegler, M. Frey, N. Neuber, G. Kumar, J. Schroers, R. Busch, and D. Cangialosi, Nat. Commun. **14**, 4698 (2023).
[7] Y. Zhao, B. Shang, B. Zhang, X. Tong, H. Ke, H. Bai, and W.-H. Wang, Sci. Adv. **8**, eabn3623 (2022).
[8] S. S. Dalal, Z. Fakhraai, and M. D. Ediger, J. Phys. Chem. B **117**, 15415 (2013).
[9] C. J. Fullerton and L. Berthier, Europhys. Lett. **119** (2017).
[10] A. Sepúlveda, M. Tylinski, A. Guiseppi-Elie, R. Richert, and M. D. Ediger, Phys. Rev. Lett. **113**, 045901 (2014).

[11] S. S. Dalal and M. D. Ediger, J. Phys. Chem. Lett. **3**, 1229 (2012).
[12] K. R. Whitaker, M. Tylinski, M. Ahrenberg, C. Schick, and M. D. Ediger, J. Chem. Phys. **143**, 084511 (2015).
[13] C. Rodríguez-Tinoco, M. Gonzalez-Silveira, J. Ràfols-Ribé, G. Garcia, and J. Rodríguez-Viejo, J. Non-Cryst. Solids **407**, 256 (2015).
[14] Y. Qiu, L. W. Antony, J. J. de Pablo, and M. Ediger, J. Am. Chem. Soc. **138**, 11282 (2016).
[15] A. Simon, O. van der Straten, N. A. Lanzillo, C.-C. Yang, T. Nogami, and D. C. Edelstein, J. Vac. Sci. Technol. A **38**, 053402 (2020).
[16] D. Sil, Y. Sulehria, O. Gluschenkov, T. Nogami, R. Cornell, A. Simon, J. Li, J. Demarest, B. Haran, C. Lavoie *et al.*, in *2021 IEEE International Interconnect Technology Conference (IITC)* (IEEE, Piscataway, NJ, 2021), pp. 1–3.
[17] P. C. Jamison, T. Tsunoda, T. A. Vo, J. Li, H. Jagannathan, S. R. Shinde, V. K. Paruchuri, and D. Gall, IEEE Trans. Electron Devices **62**, 2878 (2015).
[18] R. Rosenberg, D. Edelstein, C.-K. Hu, and K. Rodbell, Annu. Rev. Mater. Res. **30**, 229 (2000).
[19] T. Nogami, O. Gluschenkov, Y. Sulehria, S. Nguyen, B. Peethala, H. Huang, H. Shobha, N. Lanzillo, R. Patlolla, D. Sil *et al.*, in *2022 IEEE Symposium on VLSI Technology and Circuits (VLSI Technology and Circuits)* (IEEE, Piscataway, NJ, 2022), pp. 423–424.
[20] P. Luo, C. Cao, F. Zhu, Y. Lv, Y. Liu, P. Wen, H. Bai, G. Vaughan, M. Di Michiel, B. Ruta *et al.*, Nat. Commun. **9**, 1389 (2018).
[21] M. Ashby and A. Greer, Scr. Mater. **54**, 321 (2006).
[22] W. Wang, Adv. Mater. **21**, 4524 (2009).
[23] E. Flenner, L. Berthier, P. Charbonneau, and C. J. Fullerton, Phys. Rev. Lett. **123**, 175501 (2019).
[24] L. Berthier, P. Charbonneau, E. Flenner, and F. Zamponi, Phys. Rev. Lett. **119**, 188002 (2017).
[25] F. Leoni, F. Martelli, C. P. Royall, and J. Russo, Phys. Rev. Lett. **130**, 198201 (2023).
[26] D. R. Reid, I. Lyubimov, M. Ediger, and J. J. De Pablo, Nat. Commun. **7**, 13062 (2016).
[27] A. Ninarello, L. Berthier, and D. Coslovich, Phys. Rev. X **7**, 021039 (2017).
[28] L. Berthier and D. R. Reichman, Nat. Rev. Phys. **5**, 102 (2023).
[29] N. Küchler and J. Horbach, Phys. Rev. E **108**, 024127 (2023).
[30] C. Brito, E. Lerner, and M. Wyart, Phys. Rev. X **8**, 031050 (2018).
[31] H. Ikeda and F. Zamponi, J. Stat. Mech. (2019) 054001.
[32] C. Scalliet, B. Guiselin, and L. Berthier, Phys. Rev. X **12**, 041028 (2022).
[33] B. Guiselin, C. Scalliet, and L. Berthier, Nat. Phys. **18**, 468 (2022).
[34] M. Ozawa, Y. Iwashita, W. Kob, and F. Zamponi, Nat. Commun. **14**, 113 (2023).
[35] M. Ozawa, J.-L. Barrat, W. Kob, and F. Zamponi, J. Stat. Mech. (2024) 013303.
[36] G. M. Hocky, L. Berthier, and D. R. Reichman, J. Chem. Phys. **141** (2014).
[37] M. Ozawa, W. Kob, A. Ikeda, and K. Miyazaki, Proc. Natl. Acad. Sci. U.S.A. **112**, 6914 (2015).
[38] G. Kapteijns, W. Ji, C. Brito, M. Wyart, and E. Lerner, Phys. Rev. E **99**, 012106 (2019).
[39] V. F. Hagh, S. R. Nagel, A. J. Liu, M. L. Manning, and E. I. Corwin, Proc. Natl. Acad. Sci. U.S.A. **119**, e2117622119 (2022).
[40] C. Gavazzoni, C. Brito, and M. Wyart, Phys. Rev. Lett. **132**, 248201 (2023).
[41] V. Bolton-Lum, R. C. Dennis, P. Morse, and E. Corwin, arXiv:2404.07492.
[42] X. Fan, D. Xu, J. Zhang, H. Hu, P. Tan, N. Xu, H. Tanaka, and H. Tong, arXiv:2404.17675.
[43] T. Yanagishima, J. Russo, R. P. A. Dullens, and H. Tanaka, Phys. Rev. Lett. **127**, 215501 (2021).
[44] E. Sanz, C. Valeriani, E. Zaccarelli, W. C. K. Poon, M. E. Cates, and P. N. Pusey, Proc. Natl. Acad. Sci. U.S.A. **111**, 75 (2014).
[45] T. Yanagishima, J. Russo, and H. Tanaka, Nat. Commun. **8**, 15954 (2017).
[46] T. Yanagishima, J. Russo, R. P. A. Dullens, and H. Tanaka, J. Chem. Phys. **159**, 064510 (2023).
[47] M. Ruiz-Ruiz, A. Vila-Costa, T. Bar, C. Rodríguez-Tinoco, M. Gonzalez-Silveira, J. A. Plaza, J. Alcalá, J. Fraxedas, and J. Rodriguez-Viejo, Nat. Phys. **19**, 1509 (2023).
[48] A. Vila-Costa, M. Gonzalez-Silveira, C. Rodríguez-Tinoco, M. Rodríguez-López, and J. Rodriguez-Viejo, Nat. Phys. **19**, 114 (2023).
[49] C. Herrero, C. Scalliet, M. Ediger, and L. Berthier, Proc. Natl. Acad. Sci. U.S.A. **120**, e2220824120 (2023).
[50] See Supplemental Material at http://link.aps.org/supplemental/10.1103/PhysRevLett.134.128201 which includes Ref. [51], for additional details about the simulated model and supplementary analysis. The URL will become active at the time of publication.
[51] F. Leoni, H. Tanaka, and J. Russo, J. Mol. Liq. **391**, 123178 (2023).
[52] G. Wahnström, Phys. Rev. A **44**, 3752 (1991).
[53] T. Jenkinson, P. Crowther, F. Turci, and C. P. Royall, J. Chem. Phys. **147**, 054501 (2017).
[54] A. Malins, S. R. Williams, J. Eggers, and C. P. Royall, J. Chem. Phys. **139**, 234506 (2013).
[55] D. Coslovich and G. Pastore, J. Chem. Phys. **127**, 124504 (2007).
[56] U. R. Pedersen, T. B. Schrøder, J. C. Dyre, and P. Harrowell, Phys. Rev. Lett. **104**, 105701 (2010).
[57] U. R. Pedersen, I. Douglass, and P. Harrowell, J. Chem. Phys. **154**, 054503 (2021).
[58] A. P. Thompson, H. M. Aktulga, R. Berger, D. S. Bolintineanu, W. M. Brown, P. S. Crozier, P. J. in 't Veld, A. Kohlmeyer, S. G. Moore, T. D. Nguyen, R. Shan, M. J. Stevens, J. Tranchida, C. Trott, and S. J. Plimpton, Comput. Phys. Commun. **271**, 108171 (2022).
[59] E. A. Lazar, Model. Simul. Mater. Sci. Eng. **26**, 015011 (2017).
[60] W. Schirmacher, Europhys. Lett. **73**, 892 (2006).
[61] W. Schirmacher, M. Paoluzzi, F. C. Mocanu, D. Khomenko, G. Szamel, F. Zamponi, and G. Ruocco, Nat. Commun. **15**, 3107 (2024).
[62] A. Marruzzo, W. Schirmacher, A. Fratalocchi, and G. Ruocco, Sci. Rep. **3**, 1407 (2013).
[63] E. Degiuli, A. Laversanne-Finot, G. Düring, E. Lerner, and M. Wyart, Soft Matter **10**, 5628 (2014).

[64] Y. C. Hu and H. Tanaka, Nat. Phys. **18**, 669 (2022).
[65] J. Zhang and H. Zhang, and J. F. Douglas, J. Chem. Phys. **160**, 114506 (2024).
[66] T. B. Schrøder, N. Gnan, U. R. Pedersen, N. P. Bailey, and J. C. Dyre, J. Chem. Phys. **134**, 164505 (2011).
[67] X. Cao, H. Zhang, and Y. Han, Nat. Commun. **8**, 362 (2017).
[68] P. Leishangthem, A. D. S. Parmar, and S. Sastry, Nat. Commun. **8**, 14653 (2017).
[69] H. Bhaumik, G. Foffi, and S. Sastry, Proc. Natl. Acad. Sci. U.S.A. **118**, e2100227118 (2021).
[70] N. V. Priezjev, Comput. Mater. Sci. **168**, 125 (2019).
[71] T. Egami, T. Iwashita, and W. Dmowski, Metals **3**, 77 (2013).
[72] E. Bitzek, P. Koskinen, F. Gähler, M. Moseler, and P. Gumbsch, Phys. Rev. Lett. **97**, 170201 (2006).
[73] T. Egami and D. Srolovitz, J. Phys. F **12**, 2141 (1982).

End Matter

Appendix A: VHG algorithm—Here, we detail the steps of the algorithm designed to homogenize local excess pressure contributions. First, we compute the excess contributions $P_{2,i}$ of individual particles i in a glassy configuration. If $P_{2,i}$ is larger (smaller) than the mean pressure ($\overline{P_{2,i}}$), then the particle is resized by a set amount such that the pressure is reduced (increased). Whether this is an increase or decrease in particle size will depend on the derivative of the pressure with respect to σ_i. If $dP_{2,i}/d\sigma_i > 0$, then σ_i becomes $\sigma_i + \Delta\sigma$ if $P_{2,i} < \overline{P_{2,i}}$, and vice versa; if $dP_{2,i}/d\sigma_i < 0$, then the particle size corrections are reversed. The newly obtained configuration is, then, energy minimized using the FIRE algorithm [72]. If the newly obtained configuration has a decreased standard deviation in virial pressure over the whole system $\Delta P_{2,i}$, then the move is accepted and the process is repeated. If not, $\Delta\sigma$ is halved and the process repeated from the previous configuration, much like the variable step size of an optimization scheme. Typically, we start with an initial size adjustment factor $\Delta\sigma$ of 0.01. Note that $\overline{P_{2,i}}$ is recalculated after every newly accepted configuration and set of particle sizes, and the system volume is constant. The configuration is considered "converged" when five size change reductions have been carried out, but further reduction is needed to produce a configuration with a sharper $P_{2,i}$ distribution. We verified that considering more than five attempts to reduce $\Delta\sigma$ does not lead to significant further reductions in $\Delta P_{2,i}$.

Appendix B: Virial homogeneity in ultrastable systems derived from equilibration—The converse question of whether ultrastable glasses produced by other means bear the hallmarks of virial homogeneity is key to contextualizing this work, particularly whether methods based on equilibration to stabilize glasses are fundamentally related to our nonequilibrium protocol. Thus, we present preliminary analysis of the VHG nature of swap equilibrated glasses. Since direct swap equilibration of weakly polydisperse Wahnström states induce crystallization, we considered an asymmetrically polydisperse state described in previous work [27] where $p(\sigma) \sim \sigma^{-3}$ over a range $0.7253 < \sigma < 1.6095$. The density is set to $\rho^* = 1.0$. Note that the interparticle interaction is a smoothed Lennard-Jones interaction.

Applying swap to liquids and glasses at a variety of temperatures, we found that the inherent structures of equilibrated glasses at lower temperatures have significantly narrower distribution in local virial stress (see Fig. 5). This suggests that the generation of ultrastable glasses via swap equilibration spontaneously develops a homogeneity in local stress. Combined with the behavior of the VHG states, one can claim that it is a key factor underpinning their stability. We note that the relationship between the second moment of local stress and the temperature has been noted for supercooled liquids in the past, e.g., for metallic glasses [73]. The accelerated equilibration afforded by swap has allowed us to confirm this at temperatures significantly below the glass transition temperature. Thus, it is clear that virial homogenization works both ways: nonequilibrium virial homogenization can produce an ultrastable glass, but the converse also applies, i.e. that ultrastable colloidal glasses bear the key hallmark of VHG states.

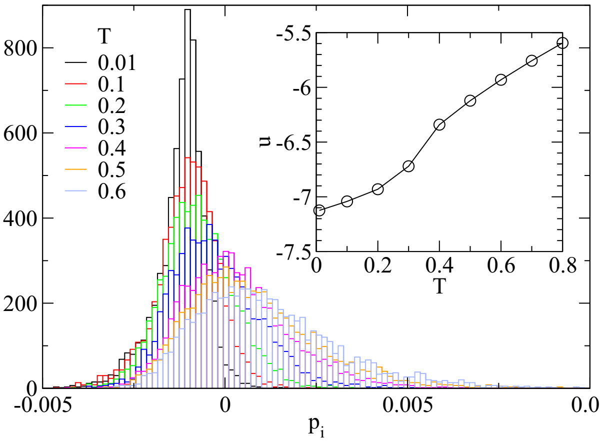

FIG. 5. Local virial stress distribution of the inherent structure of swap equilibrated glasses using a continuously polydisperse size distribution. The distributions become sharper at lower temperature. Inset: the energy of the inherent structures of the equilibrated states.